THIRTEENTH EUROPEAN ROTORCRAFT FORUM

11.5
Paper No. 67

IMPACT OF MODERN FIBER COMPOSITE MATERIALS ON DYNAMICALLY LOADED STRUCTURES

K. PFEIFER, O. HAIDER

Messerschmitt-Bölkow-Blohm GmbH, Munich, Germany

Arles, France
September, 8-11, 1987

ASSOCIATION AERONAUTIQUE ET ASTRONAUTIQUE DE FRANCE

IMPACT OF MODERN FIBER COMPOSITE MATERIALS ON DYNAMICALLY LOADED STRUCTURES

by

K. Pfeifer and O. Haider

Messerschmitt-Bölkow-Blohm GmbH, Munich, Germany

Abstract

During the last few years new composites with high-strain carbon fibers have been developed. These improved materials allow the realization of dynamically highly loaded structures such as bearingless tail rotors .

The static and dynamic performance of high-strain carbon composites are presented. Especially for load introduction elements such as springs and lugs, these materials can be of great advantage. For fiber composite structures the stresses and stiffnesses are calculated by using the unidirectional composite data. The results of the theoretical analysis are verified by component tests.

1. Introduction

Fiber composite structures are more and more used in aviation and space applications. Some of the advantages of these materials are high strength and stiffness at low weight. smooth surfaces and low crack propagation rates after impact.

To meet stiffness and strength requirements, the laminate properties can be tuned by the choice of the fiber types and by the combination of different fiber angles. Unidirectional laminates are used for carrying the longitudinal and bending loads, whereas +/-45° layers mainly transfer the torsional moments and the transverse forces because of their high shear stiffnesses.

Fiber composites are used for cowlings, empennages and even complete fuselages. Composite main and tail rotors for helicopters yield simplified designs, as the flapping and lead-lag hinges can be substituted because of the elasticity of the blade roots. For the next generation of helicopters. modern rotor concepts are being

developed. Using a flexbeam section with low torsional stiffness in the blade root, the conventional lubricated bearings can additionally be replaced. This means a big step towards cost-saving and reliable rotor systems.

This paper wants to concentrate to the properties of high-strain carbon fiber composites and their application in highly loaded helicopter components.

2. Properties of Unidirectional High-Strain CFC Laminates

For about a decade, the well known T300 fiber has been used successfully for structural parts because of its high stiffness and strength properties. During the last years, new high strain carbon fibers have been developed and put on the market. To get a comparison to T300, the properties of the following fiber types were measured with special test samples [1]:

manufacturer	designation
TORAY	T300
	T800-12 K
TOHO-ENKA	ST-3-3000
	ST-3-6000
HYSOL-GRAPHIL	E/XA-S HIGH STRAIN II6K

All samples were manufactured with the epoxy resin LY556/HT972. The same matrix system is employed in the BO 105 and BK 117 rotor blades. The properties refer to a fiber volume content of 60 %.

The designation "high-strain" for the new fibers already shows the emphasis laid on improving the strength and the strain. Therefore it is not surprising, that the Young's moduli of the examined composites have the same order of magnitude of about 140 kN/mm^2 as T300. Only T800 shows a remarkable increase of about 30% to almost 180 kN/mm^2 (Figure 1).

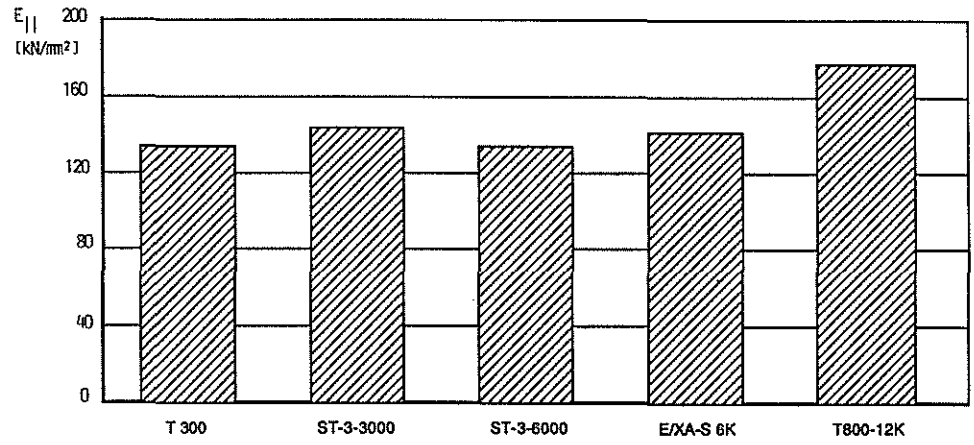

Figure 1. Young's moduli of high-strain carbon fiber composites

In Figure 2, however, the real progress of the new materials is obvious. T300 has an ultimate tensile strength of about 1600 N/mm ^{2}. All new fiber types exceed this value, having more than 2000 N/mm ^{2}. T800 has the highest strength by far with more than 3100 N/mm ^{2}. Thus the ultimate value of T300 has almost been doubled.

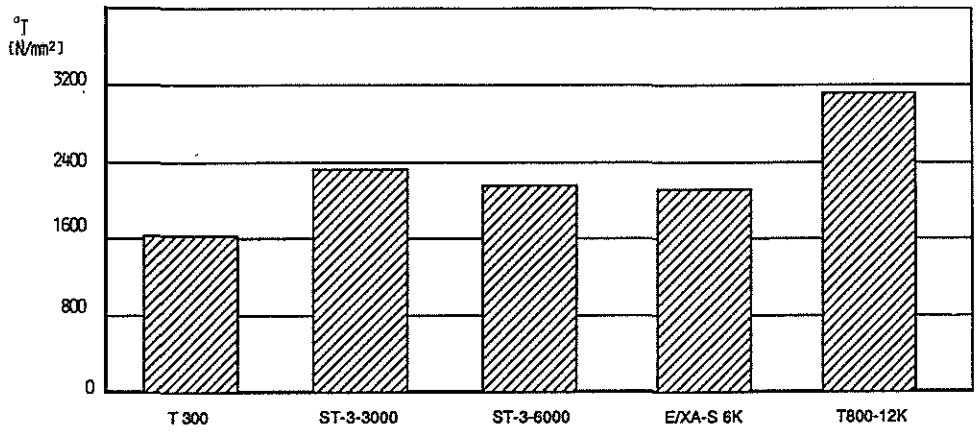

Figure 2. Ultimate tensile strength

Regarding the ultimate tensile strains in Figure 3, there are about the same relations as for the tensile strengths. The new fibers have values increased by 25 to 40 % compared to those of T300. Because of the higher Young's modulus of T800, the strain, however, does not show such a peak as the strength does.

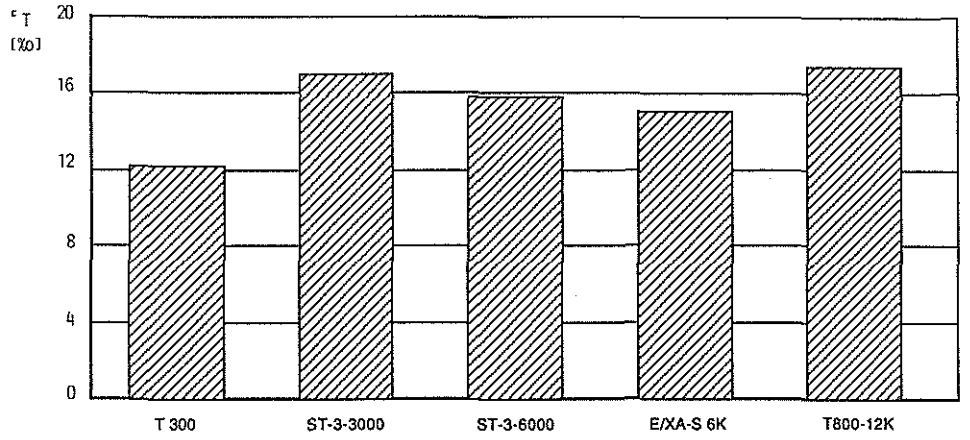

Figure 3. Ultimate tensile strain

The positive aspect of increased strength, however, cannot be confirmed for the ultimate compression strength (Figure 4). Only about 50 % of the tensile values are reached, whereas T300 has no decrease for compression. Only T800 still shows relatively good values. Therefore it must carefully be proved at the design, whether a structural part is subjected to compression loads or bending moments and whether in such a case the low compression strength doesn't defeat the advantages of high tensile strength.

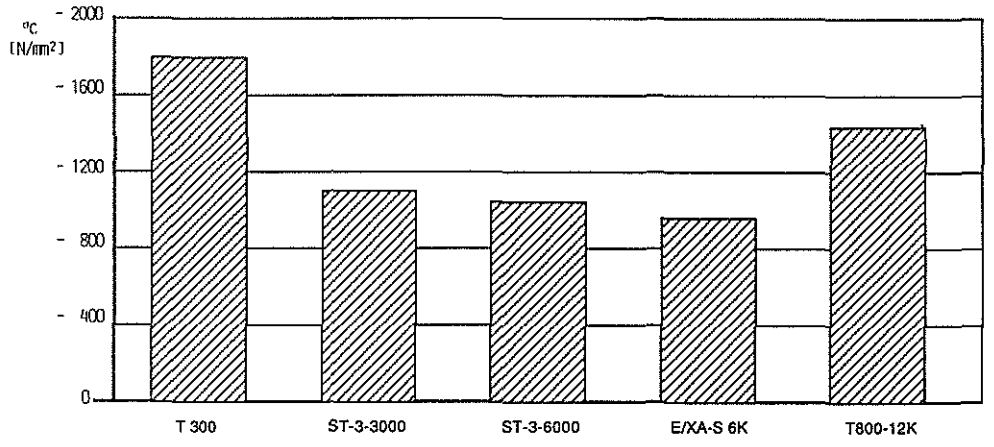

Figure 4. Ultimate compression strength

All new fiber types have almost the same ultimate interlaminar shear strength of more than 70 N/mm^2, which is little less than that of T300 (Figure 5).

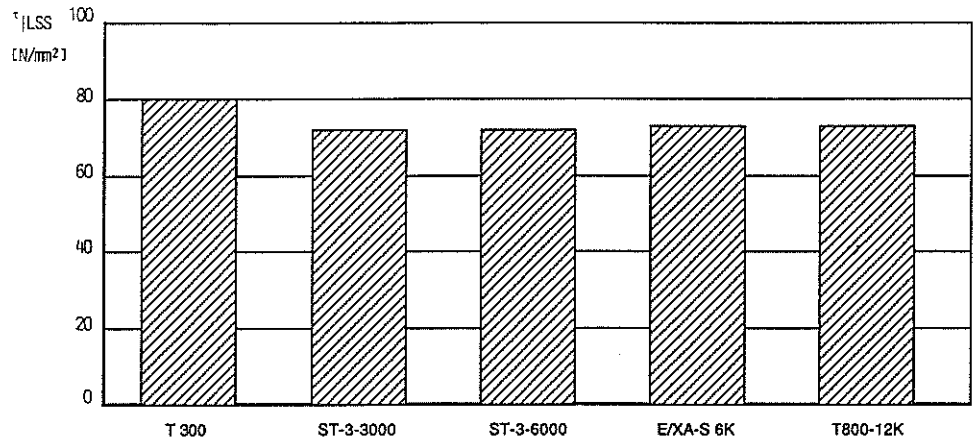

Figure 5. Ultimate interlaminar shear stress

Figure 6 shows the specific strength and stiffness characteristics of wood, metals and unidirectional composites with 60 % fiber volume content. Even if a necessary combination of different fiber angles may reduce the remarkable gap between fiber laminates and metals, the application of composites can have great advantages concerning weight and strength. The demanded stiffnesses can be reached by an appropriate choice of the fiber type.

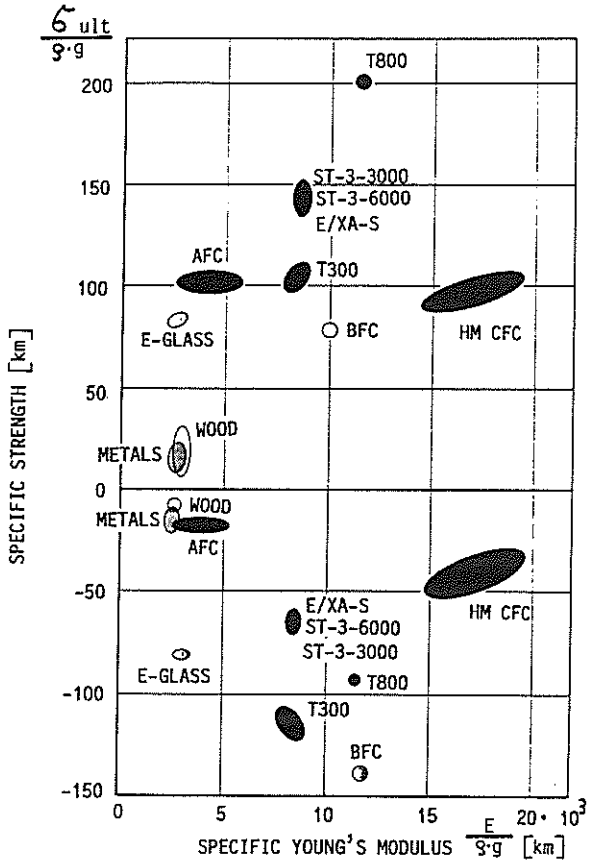

Figure 6. Specific Young's moduli and strengths of metals, wood and unidirectional composites with 60 % fiber volume content

The abbreviations mean:

GFC	glass fiber composite
AFC	aramid (trade name KEVLAR) fiber composite
BFC	boron fiber composite
HM CFC	high modulus carbon fiber composite

The new high-strain carbon fiber composites have the highest specific strengths of all shown materials with an outstanding T800. The compression strengths only reach 50 % of the tensile values.

Figure 7 shows the SN-curve for unidirectional ST-3-6000 test samples with 50 % survival probability. For infinite life, we get a stress limit of about 580 $\pm$ 380 N/mm^2 and a corresponding strain of 4.5 $\pm$ 2.8 %o. (For the design of save structures, this values, however, still must be reduced to get a sufficient survival probability.)

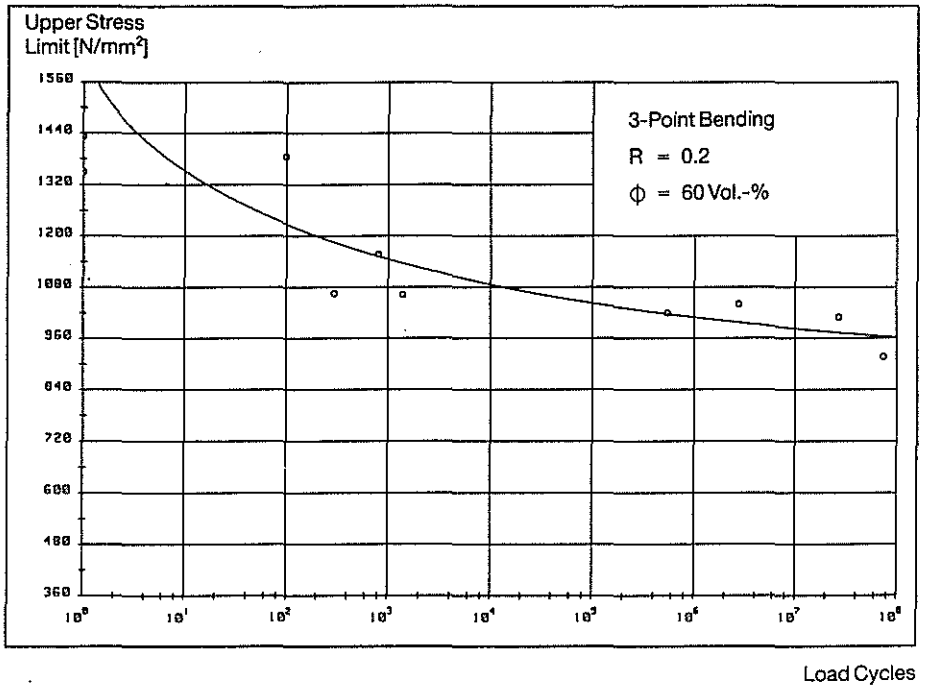

Figure 7. SN-curve for unidirectional ST-3-6000 composites

After the presentation of the high-strain fiber properties, three examples for their application shall be given in the following chapters. A bearingless tail rotor and a spring element for an anti-resonant-isolation-system have already been manufactured and tested at MBB. For composite drive shaft couplings, the use of high-strain carbon fibers can also be of great advantage.

3. Bearingless Tail Rotor

At MBB, a bearingless tail rotor has been developed for a helicopter with a maximum flight weight of about 2.5 to. During the predesign phase, the construction requirements were checked by simple formulas. A fictious flapping hinge, which is a special section of the beam with low flapping stiffness, enables the beam to provide the flapping angles. With an assumed constant curvature, this will cause a strain of:

$$\varepsilon = \frac{\sigma}{E} = \frac{\beta}{l} \cdot \frac{t}{2}$$

β = flapping angle

t = thickness

l = length

As the flapping angle is presupposed and the length shall be as short as possible, a low thickness is necessary to reduce the strain.

The pitch angles are applied by twisting the flexbeam. This causes torsional shear stresses in the laminate:

$$\tau = G \cdot \frac{\varphi}{l} \cdot t$$

φ = pitch angle

Even in this case short flexbeams can be realized only through low thickness.

For flat cross sections, however, an important aspect must be taken into account. Transverse forces in x-direction cause maximum shear stresses in the same direction at the lateral edges (Figure 8). These peaks depend on the Poisson's ratio and on the ratio of width to height. Additionally remarkable shear stresses perpendicular to the load direction occur.

Other specifications are the bending stiffnesses:

$$E\,I_{\beta} = \frac{1}{12}\,E\,a\,t^3$$

$$E\,I_{\zeta} = \frac{1}{12}\,E\,a^3\,t$$

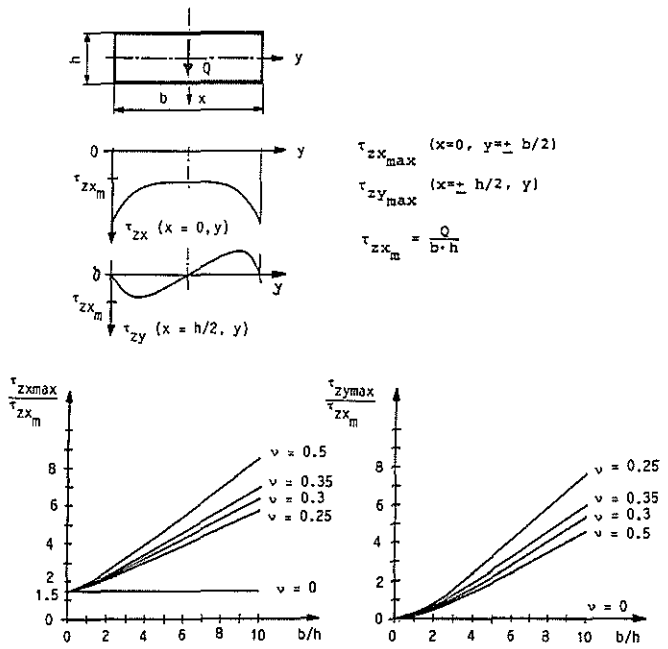

Figure 8: Shear stress distribution in isotropic beam cross sections due to transverse forces

As the rotor shall be stiff inplane, a high Young's modulus allows smaller cross sections.

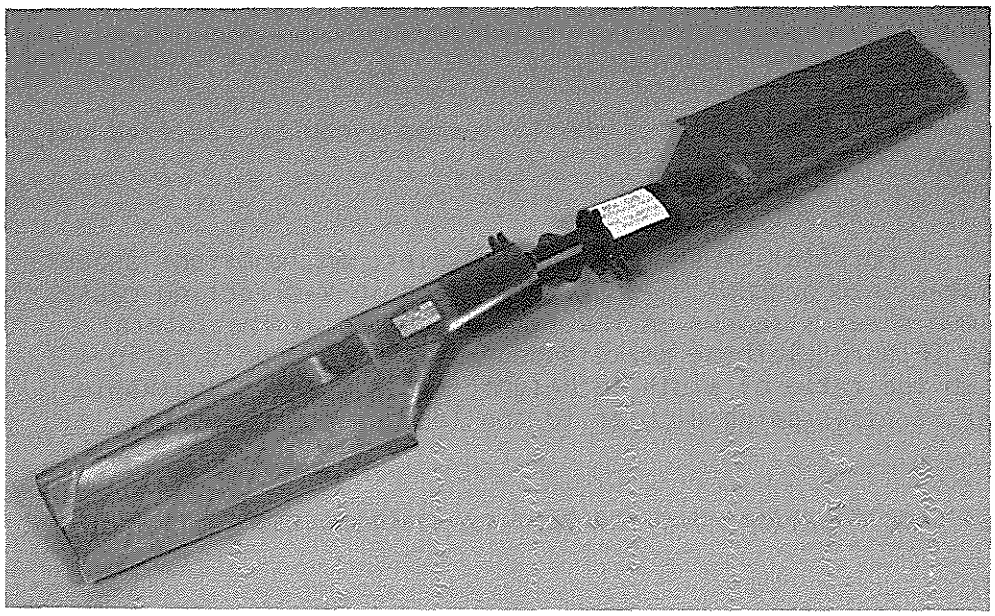

Figure 9. Bearingless composite tail rotor

These considerations led to a bearingless tail rotor with a relatively high flapping and lead-lag stiffness at the hub and with flat rectangular cross sections in the area of the flapping hinge and of the flexbeam. To sustain the high strains due to the demanded flapping angles, the carbon fiber

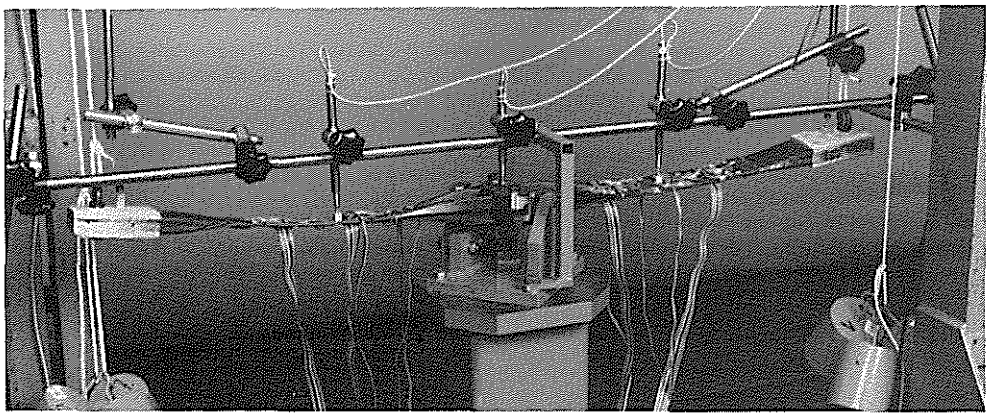

Figure 10 Flexbeam of the bearingless tail rotor during stiffness tests

The following component tests have been performed successfully:

a) Flexbeam with Flight Loads

Centrifugal force and maximum flapping and lead-lag moments; a static pitch angle of 15°
4.1×10^6 load cycles without any failure (Figure 10).

b) Start-Stop-Cycles

The test was stopped after 550 000 load cycles. No failure.

c) Dynamic loading of the pitch link and the cuff

After 10^6 load cycles the torsional stiffness was reduced by 7 % because of delaminations at the load introduction. This part, however, can be stiffened through little changes.

Summarizing it can be said, that this tail rotor will be a good solution for future helicopters.

4. Fiber Composite Coupling for Tail Rotor Drive Shafts

Drive systems consist of drive shafts and flexible couplings. These shall compensate axial and angular deviations due to manufacturing and due to the movements of the structure during operation. The use of composite couplings lead to simple designs with a lowered weight and considerably reduced number of parts (Figure 11).

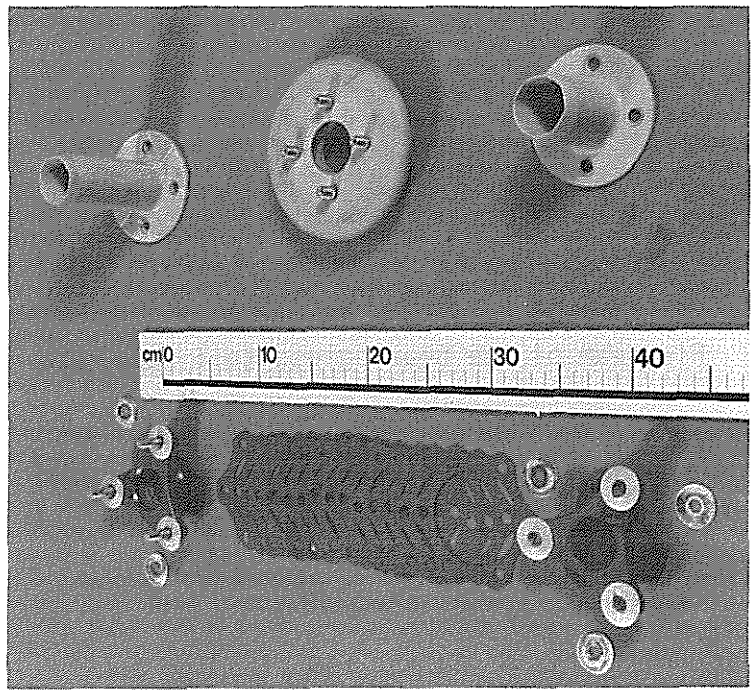

Figure 11. Comparison of the number of parts for metal and composite coupling

Couplings shall be soft regarding axial and angular movements. but shall have a high torsional stiffness to transfer the drive torque.

In a simplified way, the couplings can be considered as circular plates. Then the shear stresses due to torsion are:

$$\tau_{max} = \frac{M_T}{2\pi\, r_i^2 \cdot t}$$

t = wall thickness

r_i = inner radius

The forces due to axial displacements shall be small, as this means low axial stiffness:

$$F = k \frac{w}{r^3} Et^3$$

k = geometry factor
w = axial displacement
t = plate thickness

Also low moments due to angular movements are demanded:

$$M = k \cdot \theta \cdot Et^3$$

θ = slope angle

These formulas show, that small wall thicknesses are advantageous. To get a high torsional stiffness, a high shear modulus is needed.

Some years ago two different coupling versions were developed, a filament wound coupling with integrated flange and a press moulded prepreg coupling. The Figures 12 and 13 show the FEM idealization of both versions and the deformation of the wound coupling due to bending.(For symmetry reasons, only one half of each coupling has to be idealized.)

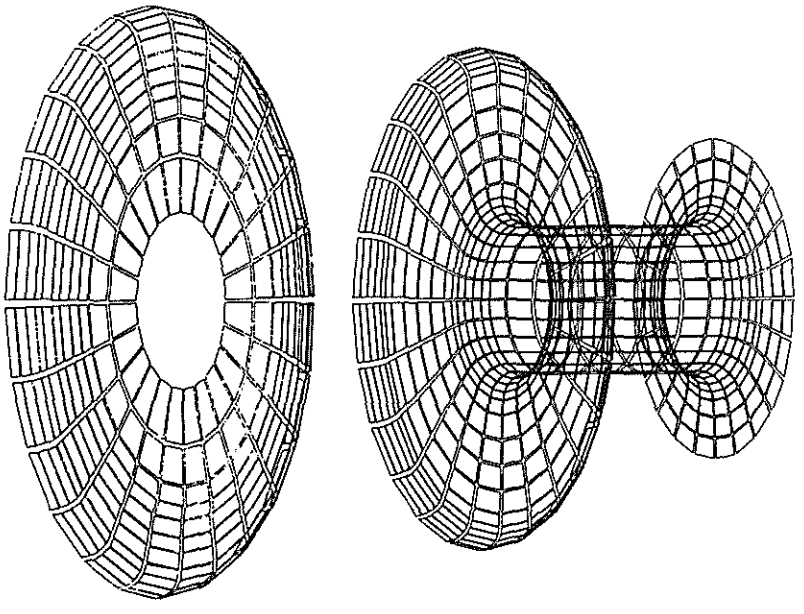

Figure 12. FEM idealization of two composite coupling versions, above filament wound, below prepreg coupling

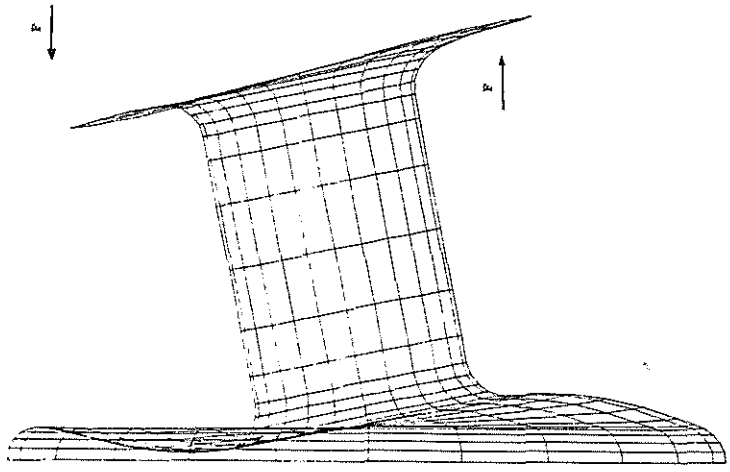

Figure 13. Bending of the filament wound coupling

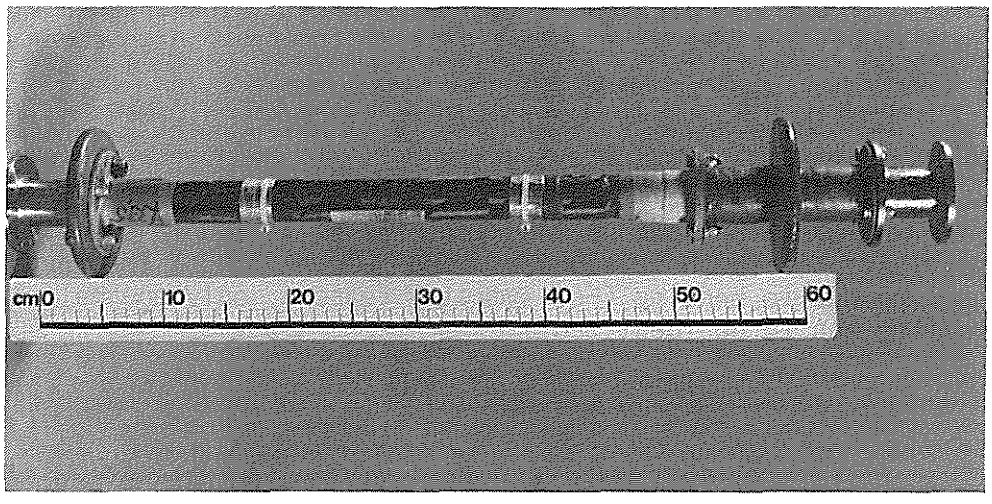

Figure 14. Test specimen with M40A drive shaft and GFC couplings

Both versions were tested together with M40A drive shafts (Figure 14). The following loads were applied:

axial elongation per coupling : 1.3 mm
angle between coupling and tube axis : 1°

Additionally different start-stop cycles including a torsional overload moment of 400 Nm were applied. Altogether 1200 flight hours were simulated without any failure of the GFC couplings. The elastic behaviour could be improved with a higher torsional and lower compression stiffness. The bending and tension stiffnesses, however, are higher in comparison with the metal version, which is a slight disadvantage. From both fiber versions the prepreg coupling showed the better results.

A package of four springs was tested. The stiffnesses in radial and axial direction were about 20 % lower than calculated. The dynamic tests were performed with a static axial displacement of 1mm and with 3 $\pm$ 1 mm in radial direction. After about 10^6 load cycles the test was stopped without any decrease in the stiffnesses. Finally the radial displacement was increased to the ultimate static load, which was reached at a displacement of 8 mm in radial direction.

In the meantime, the specifications had been changed. The demanded radial displacements are now 8 $\pm$ 1 mm, which already is the ultimate static load of the first version. Therefore the spring element has been modified. To increase the radial stiffness and strength in the area of the notches, the quasi-isotropic intermediate layers are replaced by mostly 0°/90° layers. The change to the T800 carbon fiber additionally improves the radial strength in the critical zones because of its extremely high tensile value. As the Young's modulus of T800 is about 30 % higher, we also get a positive increase of the radial and axial stiffnesses in the same order of magnitude. This allows to reduce the number of spring elements per package. The new version is being built at MBB and will be tested in the following weeks.

6. Conclusions

For more than 10 years, high tensile T300 composites have been used successfully for light-weight structures because of their high stiffness and strength. During the last years new high-strain fibers have been developed with improved tensile strengths. Their use can be of great advantage, when components are mainly loaded by high tensile stresses. The ulimate compression strengths, however, are lower than the T300 values.

At MBB, such new carbon fibers were used first for a bearingless tail rotor. This component endured the high torsion angles and normal stresses without any failure during the tests. After these encouraging results, a highly loaded spring element for an anti-resonant-isolation-system was also manufactured with these new materials.

In the future high-strain fibers will be used more and more for special applications besides the well known T300, especially since the fiber producers will continue to improve the strength and stiffness properties.

7. References

1) R. Döllinger: High-Strain-Fasern für FVW-Heckrotor
MBB-Bericht, TN-LHE244-6/85

2) H. Bansemir, W. Buchs: Component Development for Helicopter Structures
11th European Rotorcraft Forum, London, September 1985

3) C. M. Herkert, D. Braun, K. Pfeifer: CFC Drive Shaft and GFC Coupling for the Tail Rotor of the BO 105
7th European Rotorcraft and Powered Lift Aircraft Forum.
Garmisch-Partenkirchen, September 1981

4) R. Wörndle: Berechnung der Schubbeanspruchung und der Steifigkeiten von Faserverbund-Rotorblättern
DGLR Symposium, Vortrags-Nr. 87-40, Berlin 1987

Radial spring stiffness:

$$C = \frac{E}{0.3} \cdot \frac{bh^3}{12 \cdot R^3}$$

To get high radial and axial stiffnesses, there are two main possibilities. The first way is to increase the height h of the beam. This, however, also increases both the weight and the stresses and reduces the free space between the beams of the spring. Therefore it is more advantageous to use a laminate with a high Young's modulus. As this step will also cause higher bending stresses, the best solution is the use of high-strain carbon fiber composites.

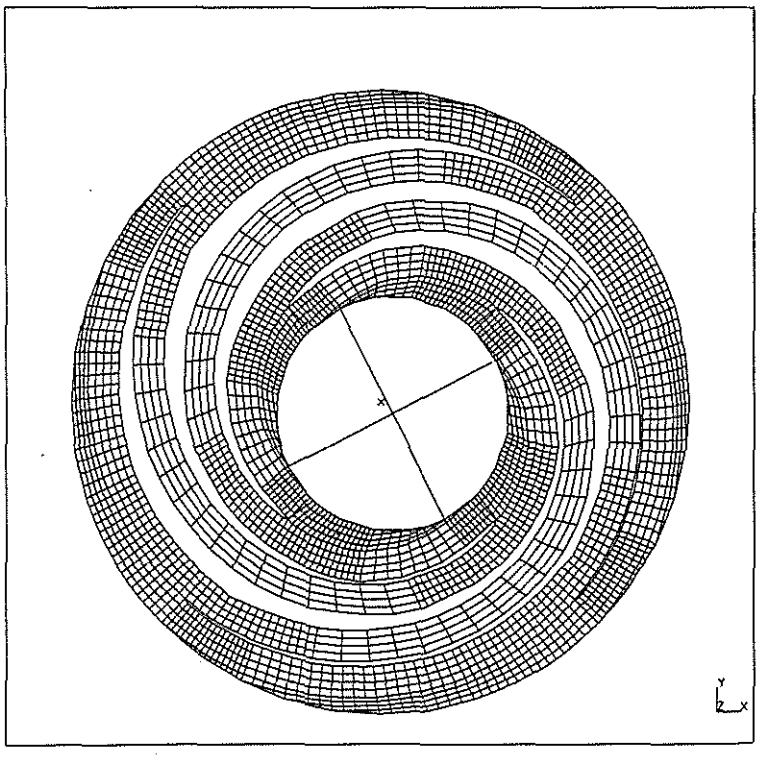

Figure 18. FEM idealization of the spring element with a radial displacement of 6 mm

Figure 18 shows a very detailed FEM NASTRAN idealization of the spring element with a radial deflection of 6 mm. In the contour plot of the circumferential stresses σ_x (Figure 19) the highest stresses occur at both ends and in an inner zone of the curved beams. The radial tension stresses σ_y, however, are much more critical because of the relatively low strength perpendicular to the fiber direction (Figure 20). These high stresses appear at both ends of the beams and are caused by the high moments in these zones and by the notches.

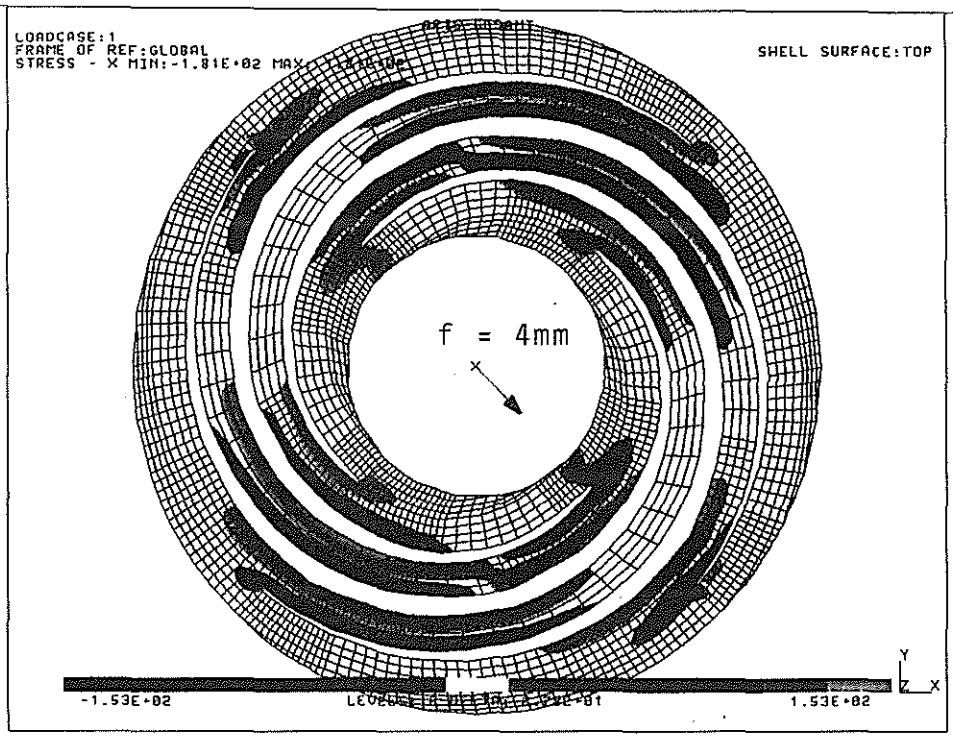

Figure 19. Circumferential stresses

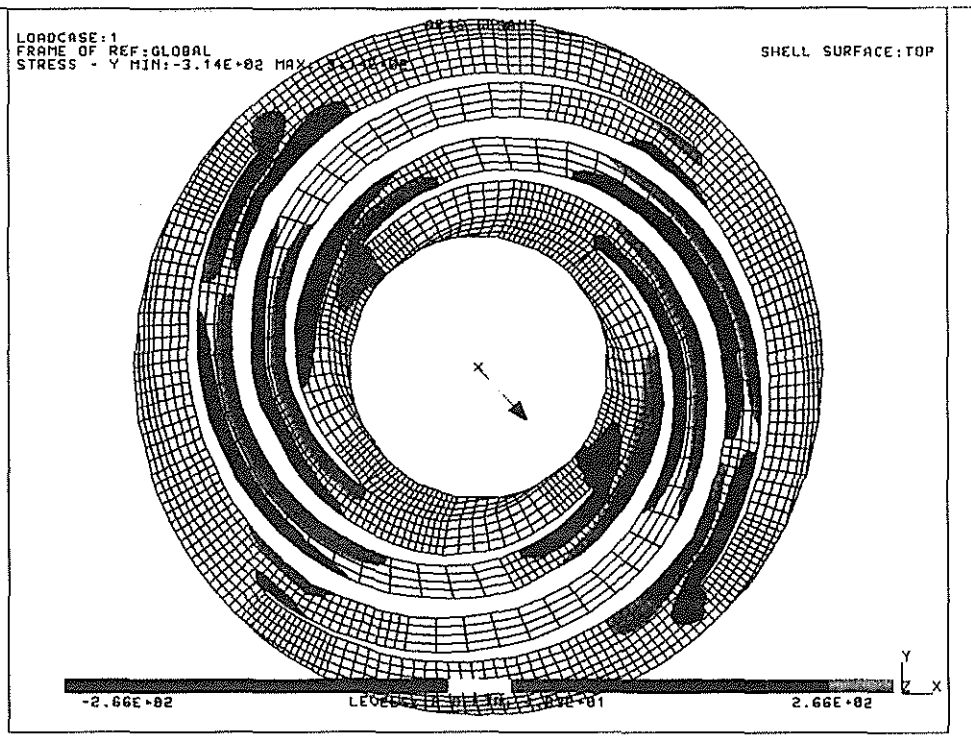

Figure 20. Radial stresses

For future application the change to CFC high strain fibers could improve the positive test results of the GFC couplings. Because of their high stiffness and strength the wall thicknesses could be reduced, gaining a further increase of torsional stiffness.

5. Spring Element for an Anti-Resonant-Isolation-System

An anti-resonant-isolation-system has been developed at MBB for a helicopter with a maximum flight weight of 5 to 6 to. Figure 15 shows a version of the complete system, which shall isolate the fuselage against the vibrations of the rotor system. Two radially stiff membranes form the center of rotation of the lever arm, whereas a package of about ten spring elements has to transfer the movements in radial direction and also the forces in axial direction.

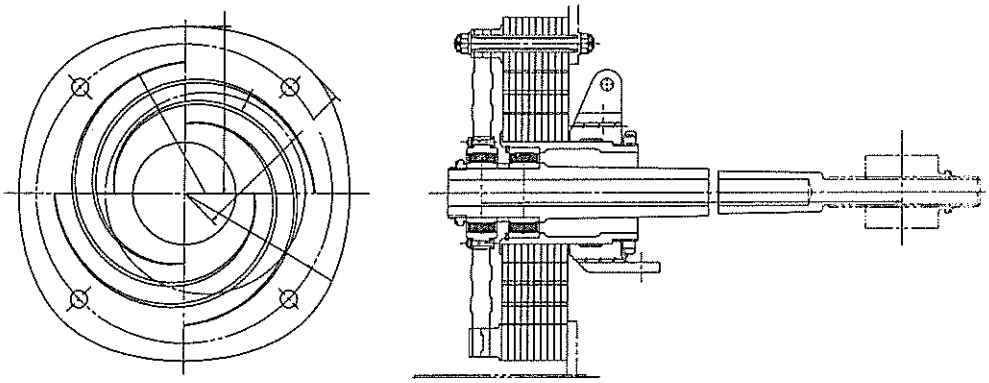

Figure 15. Version of the complete anti-resonant-isolation-system

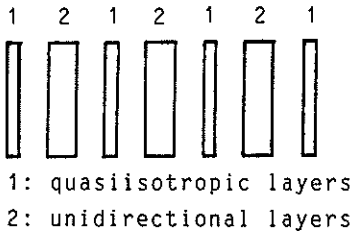

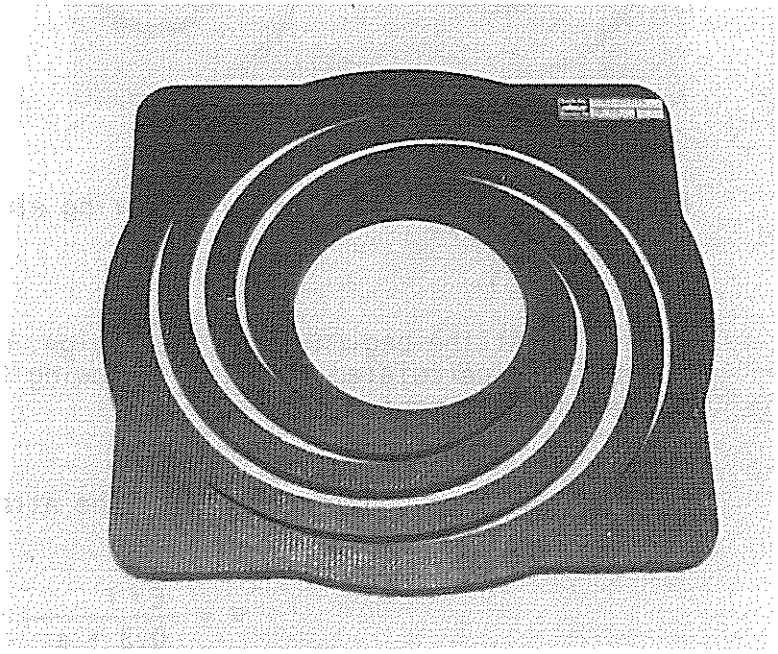

Figure 16. Spring element and laminate lay-up

Each spring element consists of 4 semicircular beams. The laminate lay-up can be seen in Figure 16. Three unidirectional ST-3-6000 packages (Figure 17) mainly yield the radial and axial stiffnesses, whereas T300 quasiisotropic intermediate layers increase the bearing and transverse strengths.

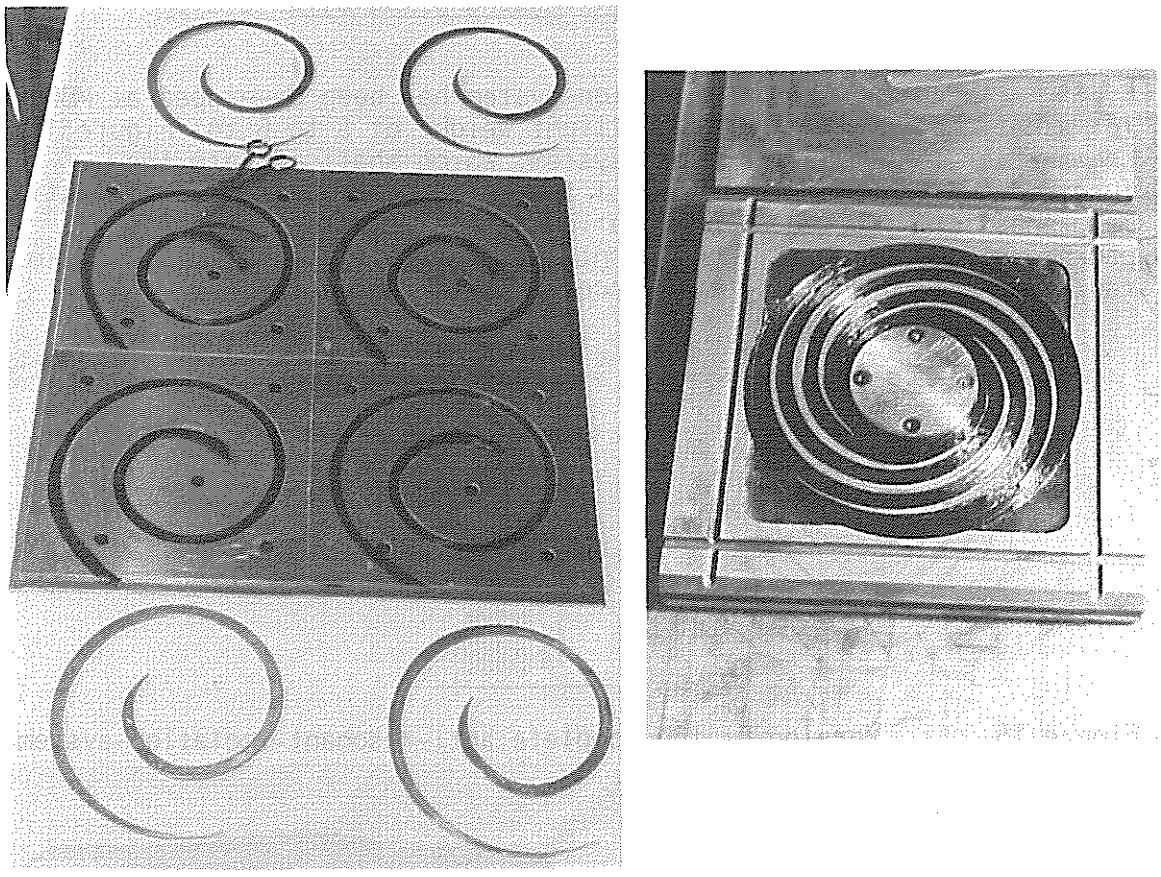

Figure 17. Manufacturing of spring element

At the beginning of the design, one beam of the spring element was calculated with the following formulas for the critical radial displacements f:

Maximum bending stress at the attachment:

$$\sigma = \frac{E \cdot f}{0.3 \cdot \pi} \cdot \frac{h}{R^2}$$